Hybridization and interference effects for localized superconducting states in strong magnetic field

A. Yu. Aladyshkin, A. S. Mel'nikov, I. M. Nefedov, D. A. Savinov, M. A. Silaev, and I. A. Shereshevskii
Institute for Physics of Microstructures RAS, 603950, Nizhny Novgorod, GSP-105, Russia
(Received 12 April 2012; published 29 May 2012)

Within the Ginzburg-Landau model, we study the critical field and critical temperature enhancement for crossing superconducting channels formed either along the sample edges or domain walls in thin-film magnetically coupled ferromagnet-superconductor bilayers. The corresponding Cooper-pair wave function can be viewed as a hybridization of two order-parameter (OP) modes propagating along the boundaries and/or domain walls. Different momenta of hybridized OP modes result in the formation of vortex chains outgoing from the crossing point of these channels. Near this crossing point, the wave functions of the modes merge, giving rise to the increase in the critical temperature for a localized superconducting state. The origin of this critical temperature enhancement caused by the wave-function squeezing is illustrated for a limiting case of approaching parallel boundaries and/or domain walls. Using both the variational method and numerical simulations, we have studied the critical temperature dependence and OP structure versus the applied magnetic field and the angle between the crossing channels.

DOI: 10.1103/PhysRevB.85.184528 PACS number(s): 74.25.Dw, 74.78.Na

I. INTRODUCTION

Recent experimental and theoretical studies of ferromagnet/superconductor (F/S) heterostructures have revealed a rich physics of magnetic and transport properties of these systems (see, e.g., Refs. 1 and 2 for review). A considerable amount of attention in these studies has been devoted to the effect of ferromagnetic domain structure on the critical temperature of superconductivity nucleation (see, e.g., Refs. 3–8 and references therein). This effect originates from both the exchange and electromagnetic (orbital) mechanisms of interaction between superconducting and magnetic orderings. The electromagnetic mechanism appears to be a dominant one for the experimental works which investigate F/S bilayers designed to suppress the proximity effect (see, e.g., Refs. 8 and 9). The nonuniform magnetic stray field of domain walls can result in the formation of a localized Cooper-pair wave function at temperatures exceeding the superconducting critical temperature in the bulk. Such localized order parameter (OP) distributions and corresponding phase diagrams have been studied in Refs. 4–6 for a generic case of a steplike profile of a stray magnetic field in a superconducting thin film. At a fixed temperature T for a certain critical amplitude B_0 $[H_{c2}(T) < B_0 \leqslant H_{c3}(T)]$ of a steplike magnetic stray field profile, the structure of localized OP wave function coincides with the one which forms in the vicinity of superconductor/vacuum or superconductor/insulator flat interface in a parallel field equal to B_0, where $H_{c2}(T)$ and $H_{c3}(T) = 1.695H_{c2}(T)$ are the critical fields of bulk superconductivity and surface superconductivity, respectively.[10]

Certainly, in a restricted sample geometry, the localized OP wave function should appear not only near the domain walls, but also at the film edges. Thus, for temperature values T between $T_{c2}(B_0)$ and $T_{c3}(B_0) > T_{c2}(B_0)$, defined by the conditions $H_{c2}(T_{c2}) = B_0$ and $H_{c3}(T_{c3}) = B_0$, respectively, there appears a set of localized superconducting modes propagating along the sample edges and/or domain walls and decaying in the transverse direction. Hereafter, these localized modes will be called superconducting channels. One can pose a natural question as to whether the superconducting critical temperature T_c could be increased due to the overlapping of the OP modes localized near the various types of superconducting channels. Indeed, such increase in the T_c value is well known to occur for two parallel superconductor/vacuum interfaces (i.e., for a superconducting film) placed in a homogeneous magnetic field H parallel to the interfaces (see, e.g., Refs. 10 and 11). The critical temperature in this system monotonously increases with the film thickness decreasing and saturates at the $T_{c0} = T_c(H = 0)$ value in the limit of small thicknesses. Taking nonparallel boundaries, we get a superconducting wedge placed in a magnetic field. The squeezing of the superconducting wave function at a small wedge angle is known to cause a strong increase in the critical temperature T_c (see Refs. 12–21).

It is the goal of our work to analyze the effect of such wave-function squeezing on the critical temperature enhancement for various types of crossing superconducting channels localized near the sample edges and/or domain walls. Within the linearized Ginzburg-Landau model, we carried out the calculations of the critical temperature of localized superconductivity for a simple hybrid system consisting of a thin superconducting film placed in a nonuniform stray magnetic field of straight domain boundaries in a ferromagnetic substrate underneath. An origin of the critical temperature enhancement can be clearly demonstrated for a generic example of parallel boundaries. Generalizing the textbook solution for the critical field of a thin superconducting film,[10,11] we consider two model problems: (i) parallel domain boundary and sample boundary separated by the distance D; (ii) two parallel domain boundaries at the separation D. In both cases, the dependence of critical temperature T_c versus the distance D reveals a maximum at the value of the order of the magnetic length $L_B = \sqrt{\hbar c/|e|B_0}$, where $\hbar$ is a Planck constant and $e = -|e|$ is an electron charge. At this distance, the wave functions of the OP modes localized near neighboring domain walls or near the domain wall and the sample edge merge and form a single superconducting channel. Turning now to the case of nonparallel domain walls (which cross at the angle $\varphi_0 \ll \pi/2$) or a domain wall crossing a sample boundary at a certain small angle φ_0, one can expect that the most

favorable conditions for superconductivity nucleation realize at the distance $\sim L_B/\varphi_0$ from the crossing point. As a result, for rather small angles $\varphi_0 \ll \pi/2$, the center of the energetically favorable OP distribution is shifted from the crossing point. This shift is accompanied by the striking phenomenon: the critical temperature T_c of the localized superconductivity monotonously increases when the tilting angle φ_0 tends to zero. Such behavior makes the dependence $T_c(\varphi_0)$ nonanalytic at $\varphi_0 = 0$ where the critical temperature exhibits a jump to the value T_{c3} (T_{c2}) for the case of the domain wall crossing the sample edge (for two crossing domain walls).

In our work, we suggest a simple variational procedure which allows us to get an approximate solution of a linearized Ginzburg-Landau equation describing the hybridization of the localized superconducting states for an arbitrary φ_0 angle. We find out that different momenta of hybridized OP modes are responsible for the formation of vortex chains outgoing from the crossing point of the channels. The effect of these chains on the OP trial function appears to be extremely important for rather large φ_0 angles close to $\pi/2$. The important effect of such vortex chain can be illustrated for the simplest example of the superconductivity nucleation at the wedge corner. Our calculations show that, only taking into account the vortex chain, one can get a proper crossover to the H_{c3} field with the increase in the wedge angle up to the flat one. The solution of a generic problem describing the superconductivity nucleation in a wedge allows us to find appropriate trial wave functions for superconducting OP nucleating near the domain walls intersecting the film edge or near the crossing point of domain boundaries. The change in the φ_0 angle is found to be accompanied by the change in the orientation of vortex chains and the intervortex distance. Our analytical findings based on the variational procedure are in a good agreement with direct numerical simulations.

By applying an external magnetic field perpendicular to the film plane, one can observe the increase in the critical temperature of the domain-wall superconductivity due to the partial magnetic field compensation inside the domains. Using both variational and numerical approaches, we have composed the phase diagram of the F/S bilayer in the plane temperature T—external magnetic field H and discuss the transitions between different superconducting states by varying temperature T, external magnetic field H, and magnetic stray field amplitude B_0.

The paper is organized as follows. In Sec. II, we mainly focus on the variational analysis of the superconductivity nucleation and interference of localized superconducting states. In Sec. III, we present the results of direct numerical simulations which support our analytical findings. Finally, the results are summarized in Sec. IV.

II. VARIATIONAL APPROACH

We start our study of the hybridization and interference effects for interacting superconducting channels forming in a thin-film magnetically coupled F/S bilayer with the Ginzburg-Landau (GL) variational procedure focusing on the analysis of appropriate trial wave functions. Let us analyze the problem of the OP nucleation in a thin superconducting film placed in the nonuniform magnetic field $\mathbf{B}(\mathbf{r}) = H\mathbf{z}_0 + \mathbf{b}(\mathbf{r})$ induced by the external sources and the magnetic domain walls in a ferromagnetic substrate, respectively. Note that we will restrict ourselves to the case of a steplike distribution of the magnetic stray fields of the domain walls and neglect the effect of the magnetic field components parallel to the film plane. In particular, for a single domain wall, we take $\mathbf{b}(\mathbf{r}) = \mathbf{z}_0 B_0 \mathrm{sign}(\widetilde{x})$, where the $\widetilde{x}$ axis is directed perpendicular to the corresponding domain wall. Thus, we neglect the deviations from this steplike field model caused by a finite thickness of a superconducting film and decay of the magnetic stray field at large distances from the domain walls (see discussion in Refs. 6, 23, and 24).

A. Linearized Ginzburg-Landau model

The superconducting critical temperature T_c can be routinely determined from the linearized GL equation

$$\left[-i\nabla - \frac{2e}{\hbar c}\mathbf{A}(\mathbf{r})\right]^2 \Psi(\mathbf{r}) = \frac{1}{\xi^2(T)}\Psi(\mathbf{r}) \tag{1}$$

as the highest possible value: $T_c = \max T$, corresponding to the lowest "energy level" $E \propto \xi^{-2}(T)$ of the eigenvalue problem (1). Here, $\Psi(\mathbf{r})$ is the OP distribution, $\mathbf{A}(\mathbf{r})$ is the vector potential corresponding to the total magnetic field $\mathbf{B}(\mathbf{r})$, m is the electron mass, and $\xi(T) = \xi_0/\sqrt{1 - T/T_{c0}}$ is the superconducting coherence length. Alternatively, T_c is known to be determined from the variational problem

$$\frac{1}{\xi^2(T)} = \frac{\int |[-i\hbar\nabla - 2e\mathbf{A}(\mathbf{r})/c]\Psi(\mathbf{r})|^2 d^2\mathbf{r}}{\hbar^2 \int |\Psi(\mathbf{r})|^2 d^2\mathbf{r}}, \tag{2}$$

and the integration is performed over the superconducting volume. The wave function $\Psi(\mathbf{r})$ satisfies the boundary condition

$$\left[-i\hbar\frac{\partial}{\partial \mathbf{n}} - \frac{2e}{c}\mathbf{A}_n(\mathbf{r})\right]\Psi(\mathbf{r})\Big|_\Gamma = 0, \tag{3}$$

where $\mathbf{n}$ is a unit vector normal to the sample boundary Γ.

The complex-valued wave function $\Psi(\mathbf{r})$ can be written in the form $\Psi(\mathbf{r}) = f(\mathbf{r})e^{i\Theta(\mathbf{r})}$, where $f(\mathbf{r})$ and $\Theta(\mathbf{r})$ are the absolute value and the phase of $\Psi(\mathbf{r})$, respectively. Thus, we can rewrite Eq. (2) in the form

$$\frac{1}{\xi^2(T)} = \frac{\int \left\{4m^2 v_s^2(\mathbf{r}) f^2(\mathbf{r}) + \hbar^2[\nabla f(\mathbf{r})]^2\right\} d^2\mathbf{r}}{\hbar^2 \int f^2(\mathbf{r}) d^2\mathbf{r}}, \tag{4}$$

where $\mathbf{v}_s(\mathbf{r}) = [\hbar\nabla\Theta(\mathbf{r}) - 2e\mathbf{A}(\mathbf{r})/c]/2m$ is a superfluid velocity.

B. Localized superconducting modes forming in the presence of parallel boundaries

We begin with the consideration of the superconductivity nucleation for parallel sample edges and/or domain walls in a thin-film F/S bilayer. Let us choose the x (y) axis to be perpendicular (parallel) to these boundaries and take the gauge $\mathbf{A} = A_y(x)\,\mathbf{y}_0$. The Schrödinger-type equation (1) does not depend on the y coordinate and one can generally find the solution in the form $\Psi(x,y) = f_k(x)\exp(-iky)$, where the function $f_k(x)$ should be determined from the following

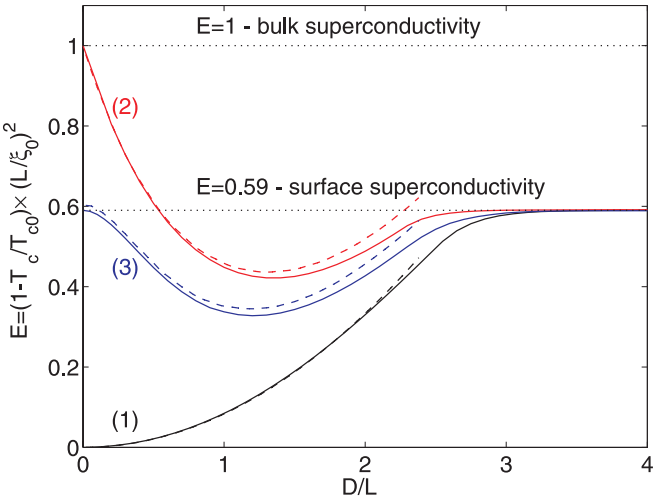

FIG. 1. (Color online) The shift of the energy $E = (1 - T_c/T_{c0})(L/\xi_0)^2$ vs the distance D, obtained numerically (solid lines) and using the trial function approach (dashed lines). The curves (1), (2), (3) correspond to three model problems: (i) two superconductor/vacuum interfaces, (ii) two domain walls, (iii) domain wall and superconductor/vacuum interface, respectively. Here, $L = L_H$ for the first problem and $L = L_B$ for the last two problems.

eigenvalue problem:

$$-\frac{d^2 f_k(x)}{dx^2} + U(x) f_k(x) = \frac{1}{\xi^2(T)} f_k(x), \qquad U(x) = \left[\frac{2\pi}{\Phi_0} A_y(x) - k\right]^2. \tag{5}$$

We calculate the dependence of the shift of the critical temperature $(1 - T_c/T_{c0})$ on the distance D using both numerical solution of the eigenvalue problem (5) and variational approach.

Two superconductor/vacuum interfaces. For two parallel superconductor/vacuum interfaces positioned at $x = \pm D/2$ and forming a superconducting slab of the finite thickness D placed in a homogeneous parallel magnetic field $B_z = H$, we should apply the boundary condition $df_k(x)/dx|_{x=\pm D/2} = 0$. The dependence of $E = (1 - T_c/T_{c0})(L_H/\xi_0)^2$ on D (where $L_H = \sqrt{\hbar c/|eH|}$ is a characteristic length scale in a magnetic field), originally calculated by Saint-James and de Gennes,[10,11] is shown in Fig. 1 by the solid line (1). The critical temperature T_c tends to T_{c0} at $D \ll L_H$ and, thus, the magnetic field has a negligible effect on the OP nucleation for rather small D values. In this limit, a simple approximation for the dependence $E(D)$ can be found provided we choose $A_y(x) = Hx$ and assume the OP wave function to be uniform across the slab. The minimum in the dependence $E(k)$ in this case corresponds to $k = 0$. Such approximation while being rigorously justified only for $D \ll L_H$ appears to describe the monotonous decrease in T_c with the increasing D distance even for $D \sim L_H$ [see the dashed line (1) in Fig. 1]. In the limit $D \gg L_H$, there are two symmetrical minima in the dependence $E(k)$ positioned at nonzero k values. These two solutions correspond to the same critical temperature T_{c3} of surface superconductivity: $T_c \simeq T_{c3} = T_{c0}(1 - 0.59|H|/H_{c2}^{(0)})$, where $H_{c2}^{(0)} = \Phi_0/2\pi\xi_0^2$ is the upper critical field at $T = 0$, and $\Phi_0 = \pi\hbar c/|e|$ is the magnetic flux quantum. The corresponding OP wave functions describe the localized superconducting modes running along the boundaries $x = -D/2$ and $D/2$.

Two domain walls. We proceed with our consideration with the case of two parallel domain walls separated by the distance D: $B_z = -B_0$ for $-D/2 \leqslant x \leqslant D/2$ and $B_z = B_0$ elsewhere (here we assume $H = 0$). In the limit $D = 0$, the critical temperature T_c equals to the bulk critical temperature $T_{c2} = T_{c0}(1 - B_0/H_{c2}^{(0)})$ in the uniform magnetic field B_0. In the opposite limiting case $D \gg L_B = \sqrt{\hbar c/|e|B_0}$, the OP wave function localized at the discontinuities of the magnetic field component B_z saturates the critical temperature T_{c3}. What is less intuitively clear is that the transition from T_{c2} to T_{c3} with the increasing distance D occurs via the T_c enhancement. Such nonmonotonous T_c behavior can be captured with a good accuracy by minimizing the energy functional (4) for the Gaussian-type trial function: $f_k(x) = \exp(-x^2/a^2)$, where a is a variational parameter. The choice $A_y(-x) = -A_y(x)$ automatically yields $k = 0$. Then, it is clear that the rise in T_c is caused by the increase in the width of the effective potential well $U(x) = A_y^2(x)$ for increasing D and by the lowering of the ground energy level in a wider potential well. The comparison of the results of the numerical solution of Eq. (5) [solid line (2)] with the trial function approach [dashed line (2)] is presented in Fig. 1.

Domain wall and superconductor/vacuum interface. Finally, we analyze the case of a single domain wall parallel to the superconducting film edge and positioned at a distance D from this edge. We also assume $H = 0$ so that the only characteristic length scale is L_B. Similarly to the previous case, the T_c value changes nonmonotonously as a function of D, and in both limits ($D \ll L_B$ and $D \gg L_B$) the critical temperature tends to the critical temperature of surface superconductivity: $T_c \to T_{c3}$. At $D \to \infty$, there are two independent superconducting OP nuclei located near the surface ($x = -D/2$) and at the domain wall ($x = D/2$), both characterized by the same critical temperature T_{c3}. Analogously to the previous case of two parallel domain walls, the nonmonotonous behavior of T_c is caused by the increasing width of the potential well $U(x) = [2\pi A_y(x)/\Phi_0 - k]^2$ in Eq. (5). The problem can be apparently mapped on the one in the infinite superconducting slab in the magnetic field of three parallel domain walls placed at $x = \pm D/2$ and $-3D/2$. The resulting magnetic field distribution is an odd function for reflection respective to the plane $x = -D/2$. For such magnetic field configuration, the ground-state solution should possess the reflection symmetry: $f_k(x - D/2) = f_k(-x - D/2)$. Therefore, for $D \leqslant L_B$, we can choose the trial function in the form $f_k(x) = \exp[-(x - D/2)^2/a^2]$, where a is a variational parameter. Unlike the previous case, the vector potential now is an even function $A_y(x + D/2) = A_y(-x - D/2)$, which means that the ground-state solution corresponds to $k \neq 0$. Minimizing the energy functional over the parameters a and k, we obtain the shift of the critical temperature shown by dashed line (3) in Fig. 1. This plot again demonstrates an excellent agreement with the numerical result [solid line (3)] for rather small D values. Thus, the solution of these model problems allows us to make an important observation about

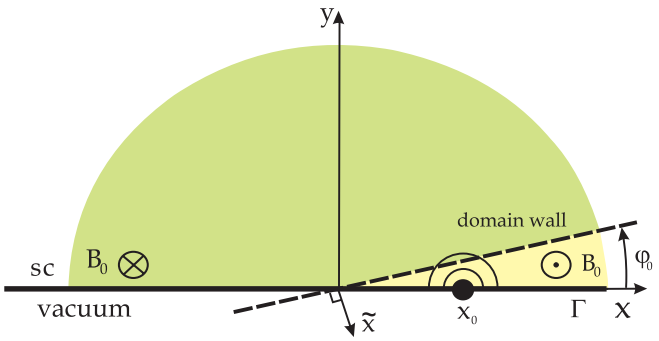

FIG. 2. (Color online) Schematic view of a F/S bilayer: a semi-infinite thin superconducting film and a straight domain wall (dashed line) oriented at a certain angle $\varphi_0 \ll \pi/2$ with respect to the film edge Γ. B_0 is a stray field amplitude inside the domain.

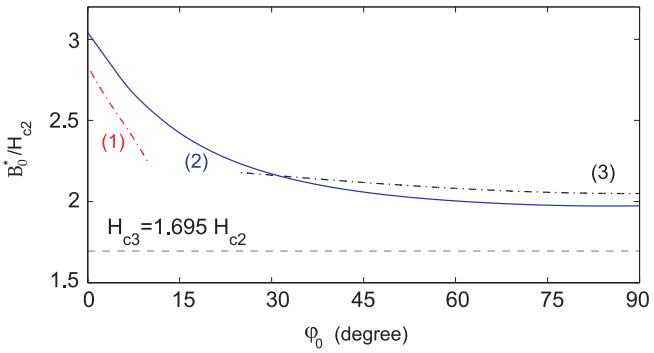

FIG. 3. (Color online) The critical amplitude B_0^* of the domain stray field of localized superconductivity nucleation in a thin-film semi-infinite F/S bilayer as a function of the titling angle φ_0. Dashed-dotted lines (1) and (3) are obtained from the variational analysis carried out both for small and large corner angles, respectively. The dependence $B_0^*(\varphi_0)$ found from numerical simulations is shown by the solid line (2).

the possibility to get the critical temperature enhancement for a pair of approaching boundaries or domain walls.

C. Hybridization of localized superconducting modes propagating along the channels crossing at small angles

Considering the problem of superconductivity nucleation for crossing boundaries or domain walls, it is natural to start from the simplest case of small crossing angles when the distance D between the crossing boundaries changes adiabatically.

Two superconductor/vacuum interfaces. The solution for two crossing superconductor/vacuum interfaces which form a superconducting wedge with small corner angle $\chi \ll \pi/2$ can be found in Refs. 12–21. Let us introduce a cylindrical coordinate system (r,φ,z). The monotonous increase in T_c with the decreasing distance D discussed above allows us to assume that the maximum of the OP wave function should be positioned at the wedge vertex ($r = 0$). Substituting the simplest isotropic wave function $\Psi(\mathbf{r}) = \exp(-r^2|eH|\chi/2\sqrt{3}\hbar c)$ in the functional (2) and carrying out the variational procedure, one can find the following asymptotical expression for the critical magnetic field $H_{c3}^{\mathrm{w}} \simeq \sqrt{3}H_{c2}/\chi$ suppressing the localized superconductivity.

Domain wall crossing the superconductor/vacuum interface. We proceed now with the case of a single domain wall oriented at a rather small angle φ_0 with respect to the superconducting film edge Γ (see Fig. 2). We restrict ourselves by a particular case of zero external field $H = 0$. Thus, we consider the variational problems, Eqs. (2) and (3), for a semi-infinite superconducting thin film in a magnetic stray field $b_z(\mathbf{r}) = B_0\mathrm{sign}(\tilde{x})$. We choose the trial function $f(\mathbf{r})$ in the form

$$f(\mathbf{r}) = e^{-\delta y^2} e^{-\beta(x-x_0)^2}, \tag{6}$$

where δ, β, and x_0 are the variational parameters. Here, we allow the center of a superconducting nucleus to be shifted from the crossing point of the domain wall and the sample edge Γ only along the x axis ($x_0 \neq 0$). The shift of the nucleus center is a direct consequence of the existence of the maximum in the dependence of the critical temperature T_c versus the separation D between the boundaries. According to the above treatment, this maximum corresponds to the D value of the order of the magnetic length L_B. Thus, for a small angle φ_0, the peak in the OP wave function should appear at the distance $\sim L_B/\varphi_0$ from the crossing point.

Accounting for the magnetic stray field $b_z(\mathbf{r})$ of the domain wall, we take the superfluid velocity $\mathbf{v}_s(\mathbf{r})$ in each magnetic domain to be equal to the vector potential $\mathbf{A}(\mathbf{r})$ chosen in the radial gauge:

$$\begin{aligned} \mathbf{v}_s(\mathbf{r}) &= B_0 r(\varphi - \vartheta) \times |e|/(mc)\,\mathbf{r}_0, \quad 0 \leqslant \varphi < \varphi_0 \\ \mathbf{v}_s(\mathbf{r}) &= B_0 r(-\varphi + 2\varphi_0 - \vartheta) \times |e|/(mc)\,\mathbf{r}_0, \quad \varphi_0 < \varphi \leqslant \pi \end{aligned} \tag{7}$$

where ϑ is the variational parameter ($0 \leqslant \vartheta \leqslant \varphi_0$).

Substituting the expressions (6) and (7) into Eq. (4) and carrying out the minimization over the parameters δ, β, x_0, and ϑ, we derive the dependence of the critical field amplitude B_0^* versus the φ_0 angle for the limit of small angles $\varphi_0 \ll 1$. The typical plot of this dependence is shown in Fig. 3 by a dashed-dotted line (1). For $\varphi_0 \ll 1$, this plot demonstrates a good agreement with our numerical simulations [see the solid line (2) in Fig. 3] carried out in the following. It is interesting to note that the position x_0 of the OP maximum diverges inversely proportional to φ_0 as $\varphi_0 \to 0$ in accordance with our expectation [see Fig. 4(a)]. The parameter δ is found to be independent of φ_0: $\delta = 0.16\xi_0$. The dependencies of the variational parameters β and ϑ versus the φ_0 angle are presented in Fig. 4(b).

One can see that even for $\varphi_0 \ll 1$, the critical field B_0^* differs from the H_{c3} value corresponding to conventional surface superconductivity in a homogeneous field: $B_0^* \to 2.8H_{c2}$ at $\varphi_0 \to 0$. At $\varphi_0 = 0$, the dependence $B_0^*(\varphi_0)$ exhibits a steplike jump to the H_{c3} field. This jump should be, of course, smeared for a finite-size sample when x_0 becomes comparable to the sample size. It is important to note that the threshold value B_0^* allows us to determine the critical temperature at $H = 0$: $T_c = T_{c0}\,(1 - B_0/B_0^*)$.

Two domain walls. The consideration in previous sections can be easily generalized for the case of two domain walls which cross at rather small angle $\varphi_0 \ll \pi/2$ (see Fig. 5). Due to the symmetry of the magnetic field distribution, we can consider only the half-space: $0 \leqslant \varphi \leqslant \pi$. We take the

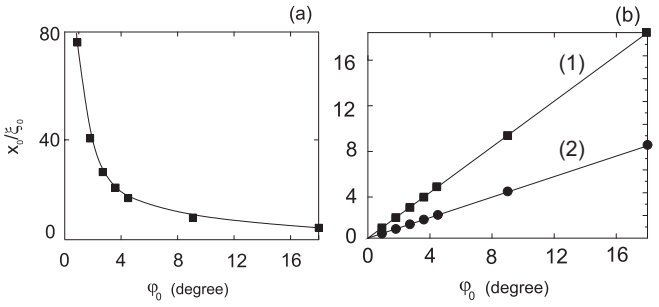

FIG. 4. (a) Variational parameter x_0 vs φ_0 obtained using the trial function approach (squares). The solid line corresponds to the analytical dependence $x_0 = 72^\circ/\varphi_0$. (b) The dependencies of $\beta \times 180^\circ$ (squares) and ϑ (circles) vs φ_0 obtained using the trial function approach. The solid lines (1) and (2) correspond to the analytical dependencies $\beta \times 180^\circ = \varphi_0$ and $\vartheta = \varphi_0/2.2$, respectively.

superfluid velocity $\mathbf{v}_s(\mathbf{r})$ in the form (7) and choose the trial function $f(\mathbf{r})$ as in the following:

$$f(\mathbf{r}) = e^{-\delta(y-y_0)^2} e^{-\beta(x-x_0)^2}. \tag{8}$$

Here, δ, β, x_0, and y_0 are the variational parameters. It is important to note that the center of a superconducting nucleus is shifted from the crossing point of two domain walls along both the x and y axes. Substituting the expressions (7) and (8) into Eq. (4) and carrying out the minimization over the parameters δ, β, x_0, y_0, and ϑ, we derive the dependence $B_0^*(\varphi_0)$ for the limit of small angles $\varphi_0 \ll 1$. This critical field dependence appears to be very close to the one shown in Fig. 3 by the dashed-dotted line (1): the relative deviation is of the order of several percent. We emphasize that the nucleus center (x_0, y_0) shifts along the bisectrix of the φ_0 angle.

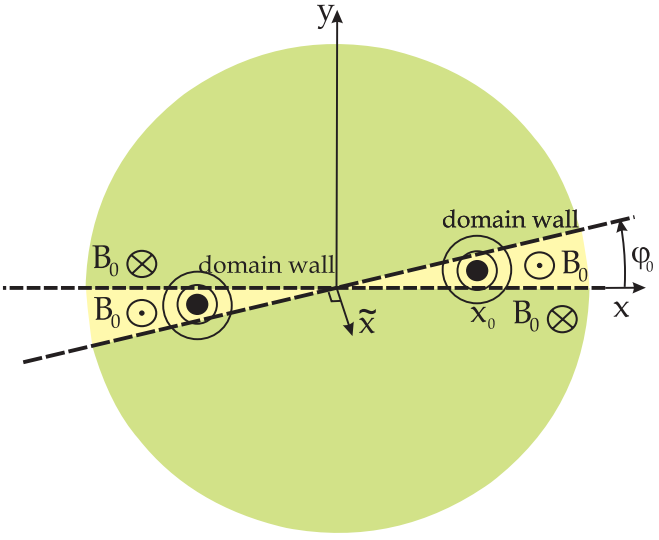

FIG. 5. (Color online) Schematic view of a F/S bilayer: a thin superconducting film and two domain walls (dashed lines) crossing at a certain angle $\varphi_0 \ll \pi/2$. B_0 is a stray field amplitude inside the domain.

D. Interference of localized superconducting modes propagating along the channels crossing at large angles

We proceed now with the consideration of the localized superconductivity nucleation for the superconducting channels crossing at rather large angles.

Two superconductor/vacuum interfaces. We start with an exemplary problem of superconductivity nucleation in a wedge with the corner angle $\chi \leqslant \pi$ placed in a uniform magnetic field H. The superconducting wave function localized near the wedge vertex can be considered as an overlapping of the superconducting modes propagating along the wedge sides. These modes are characterized by the wave vectors parallel to the different sides and, thus, the interference of these localized waves should result in a formation of vortices at the bisectrix of the wedge angle. The superconductivity in a wedge appears for $H > H_{c3}$ and, thus, the OP decays with the increasing distance from the wedge vertex. We would like to note that the interference effect and the resulting formation of a vortex chain have been disregarded in previous works[12–16,22] considering different types of trial functions for the OP in a wedge. As a consequence, all these variational calculations provided poor agreement with the numerical results (see, e.g., Ref. 18) for rather large wedge angles up to π. We will demonstrate that only by accounting for the vortex chain outgoing from the wedge vertex one can obtain a proper crossover to the H_{c3} field at $\chi \to \pi$.

Considering a superconducting wedge (see Fig. 6) and introducing the dimensionless variables in the functional (4), we come to the following expression:

$$\frac{1}{h} = \frac{\int \left\{\mathbf{v}_s'^2(\mathbf{r}')f^2(\mathbf{r}') + [\nabla f(\mathbf{r}')]^2\right\} d^2\mathbf{r}'}{\int f^2(\mathbf{r}')d^2\mathbf{r}'}, \tag{9}$$

where $h^{-1} = L_H^2/\xi_0^2(1 - T/T_{c0})$, $d^2\mathbf{r}' = L_H^{-2}d^2\mathbf{r}$, $\mathbf{v}_s'(\mathbf{r}') = \nabla\Theta(\mathbf{r}') + a(\mathbf{r}')$ is a dimensionless superfluid velocity, and $a(\mathbf{r}') = |H|^{-1}\mathbf{A}(\mathbf{r}')$ is a dimensionless vector potential.

Similarly to Ref. 14, we choose the absolute value $f(\mathbf{r}')$ of Cooper-pair wave function $\Psi(\mathbf{r}')$ in the form

$$f(\mathbf{r}') = \exp\{-\alpha r'^2[1 + \gamma \sin^2(\pi\phi/\chi)]\}, \tag{10}$$

where α and γ are the variational parameters, $r' = L_H^{-1}r$, and $\phi = \varphi - \chi/2$. To describe the vortex chain positioned along

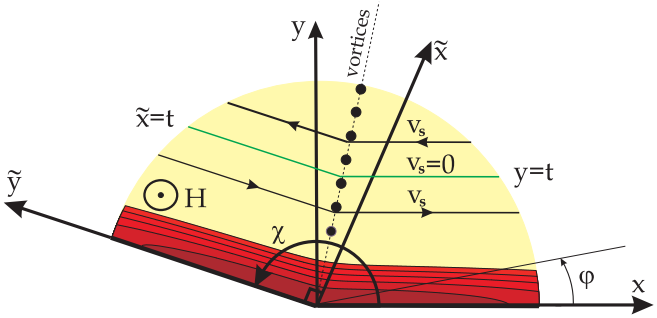

FIG. 6. (Color online) Cross section of a superconducting wedge with an arbitrary corner angle χ in a uniform magnetic field H. The solid circles show the vortex chain outgoing from the wedge vertex along its bisectrix. The lines of a superfluid velocity $\mathbf{v}_s$ and the contour lines of $f(\mathbf{r})$ are presented. Dashed lines ($\tilde{x} = t$ and $y = t$) correspond to $\mathbf{v}_s = 0$.

the bisectrix, we introduce a cut along the line $\phi = 0$ where the superfluid velocity experiences a discontinuity. The tangential jump in the v_s value corresponds to a continuously distributed vorticity along this cut. For this purpose, we divide the wedge into the angular domains $-\chi/2 \leqslant \phi < 0$ and $0 \leqslant \phi \leqslant \chi/2$ and take the dimensionless superfluid velocity $v_s'(\mathbf{r}')$ in each domain equal to the vector potential $a(\mathbf{r}')$ chosen parallel to the wedge sides at $\phi = \mp\chi/2$, correspondingly. Both gauges of the vector potential $\mathbf{a}(\mathbf{r}')$ correspond to a uniform field $\mathbf{H}$:

$$\begin{aligned} \mathbf{v}_s'(\mathbf{r}') &= (t - y')\,\mathbf{x}_0\,, \quad -\chi/2 \leqslant \phi < 0 \\ \mathbf{v}_s'(\mathbf{r}') &= (\widetilde{x} - t)\,\widetilde{\mathbf{y}}_0\,, \quad 0 \leqslant \phi \leqslant \chi/2 \end{aligned} \tag{11}$$

where t is a variational parameter, and $(\widetilde{x},\widetilde{y})$ is a new reference system rotated at the angle $\chi - \pi/2$ with respect to the original system (x,y) in the counterclockwise direction (see Fig. 6). Such choice of the superfluid velocity provides a correct asymptotical behavior of the OP modes propagating along different wedge sides at large distances from the vertex. Of course, a single-valued wave function should vanish at the cut and, thus, the choice of superfluid velocity in the form Eq. (11) is not adequate for description of the wave-function behavior close to the wedge vertex ($r \lesssim \xi$) where the absolute value of the OP is essentially nonzero for all angles ϕ. As a consequence, we can use this method only for wave functions strongly elongated along the wedge sides when the region close to the vertex provides a small contribution to the functional (9). We will see in the following that this condition appears to break down for small angles χ when the wave function is almost isotropic for all distances r.

By rewriting the expressions (11) in terms of r' and ϕ and substituting them into Eq. (9), one obtains the function $h^{-1} = h^{-1}(\alpha,\gamma,t,\chi)$. By carrying out the minimization over the variational parameters α, γ, and t, we find the critical field $H_{c3}^{\mathrm{w}}(T) = H_{c2}(T) \times [\min_{\alpha,\gamma,t}(1/h)]^{-1}$ of superconductivity nucleation for different wedge angles χ. A typical plot of the dependence $H_{c3}^{\mathrm{w}}(\chi)$ is presented in Fig. 7 by the solid line.

One can see that for $\chi = \pi$, we obtain the result found previously by Saint-James and de Gennes:[10] $H_{c3}^{\mathrm{w}}(\pi) \simeq 1.695 H_{c2}$. For a particular case $\chi = \pi/2$, we find $H_{c3}^{\mathrm{w}}(\pi/2) \simeq 2H_{c2}$. This value appears to be in a good agreement with the numerical calculations carried out in Ref. 18 (see also the comparison with numerical simulations below). The variational parameters corresponding to this case should be taken as follows: $\alpha(\pi/2) = 0.14$, $\gamma(\pi/2) = -0.5$, $t(\pi/2) = 0.6$.

By analyzing the typical contour plots of the $f(\mathbf{r}')$ function in the insets of Fig. 7 for different χ, one can see that the angular anisotropy of the OP vanishes ($\gamma \to 0$) in the limit $\chi \to 0$. For such small angles χ, we find $H_{c3}^{\mathrm{w}}/H_{c2} \simeq 1.56\sqrt{3}\,\chi^{-1}$. This asymptotical behavior deviates from the correct dependence $H_{c3}^{\mathrm{w}}/H_{c2} = \sqrt{3}\,\chi^{-1}$ found previously in Refs. 12–21. This deviation for small angles is a natural consequence of the wave-function isotropy as it is discussed above. With the increase in the wedge angle χ, the anisotropy parameter $|\gamma|$ grows and the wave function becomes elongated along the wedge sides, which restores the validity of our approach. The vortex-free trial functions considered in Refs. 12–16 and 22 can no more provide a correct behavior of the upper critical field H_{c3}^{w}.

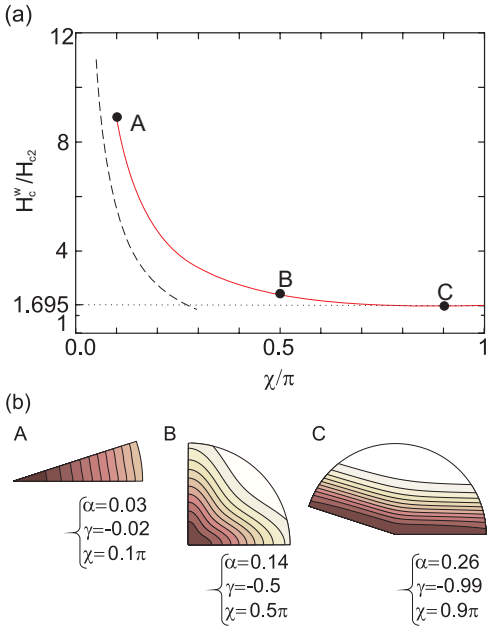

FIG. 7. (Color online) (a) Typical plots of the nucleation field H_{c3}^{w} in a wedge vs the corner angle χ. The solid line shows the results of our variational calculations, while the dashed line corresponds to asymptotic behavior of the nucleation field H_{c3}^{w} at small corner angles $\chi \ll 1$ according to Refs. 12–21. (b) The contour plots of $f(\mathbf{r}')$ function inside the areas $r' \leqslant 5$ for different χ angles: 0.01π (A), 0.5π (B), and 0.9π (C).

Domain wall crossing the superconductor/vacuum interface. The variational procedure described in the latter section can be easily generalized for other model systems containing crossing superconducting channels. We proceed now with the consideration of the localized superconductivity nucleation in a thin-film semi-infinite F/S bilayer with a domain wall crossing the sample edge Γ at rather large angle $\varphi_0 \leqslant \pi/2$ (see Fig. 8). To generalize the considered approach, one needs to introduce two vortex chains outgoing from the crossing point of a domain wall and the sample edge Γ. It is natural to expect these vortex chains to be oriented along the bisectrices of two wedge-shaped regions located to the left and to the right of the domain wall. We follow the procedure described in the previous section and replace the vortex chains by the cuts for superfluid velocity, i.e., by the lines with a continuously distributed vorticity. The absolute value of the OP wave function and the dimensionless superfluid velocity are taken in the forms

$$\begin{aligned} f_1(\mathbf{r}) &= \exp\{-\alpha_1 r^2[1 + \gamma_1 \cos^2(\pi\varphi/\varphi_0)]\}, \quad 0 \leqslant \varphi < \varphi_0 \\ f_2(\mathbf{r}) &= \exp\{-\alpha_2 r^2[1 + \gamma_2 \cos^2(\pi(\varphi - \varphi_0)/(\pi - \varphi_0))]\}, \\ &\qquad \varphi_0 \leqslant \varphi \leqslant \pi \end{aligned} \tag{12}$$

$$\begin{aligned} \mathbf{v}_s(\mathbf{r}) &= (H + B_0)(\eta - y) \times |e|/(mc)\,\mathbf{x}_0, \quad 0 \leqslant \varphi < \varphi_0/2 \\ \mathbf{v}_s(\mathbf{r}) &= (H + B_0)(\widetilde{x} - \eta) \times |e|/(mc)\,\widetilde{\mathbf{y}}_0, \quad \varphi_0/2 \leqslant \varphi < \varphi_0 \\ \mathbf{v}_s(\mathbf{r}) &= (H - B_0)(\widetilde{x} + \eta) \times |e|/(mc)\,\widetilde{\mathbf{y}}_0, \\ &\qquad \varphi_0 \leqslant \varphi < \pi/2 + \varphi_0/2 \\ \mathbf{v}_s(\mathbf{r}) &= (H - B_0)(\eta - y) \times |e|/(mc)\,\mathbf{x}_0, \\ &\qquad \pi/2 + \varphi_0/2 \leqslant \varphi \leqslant \pi \end{aligned} \tag{13}$$

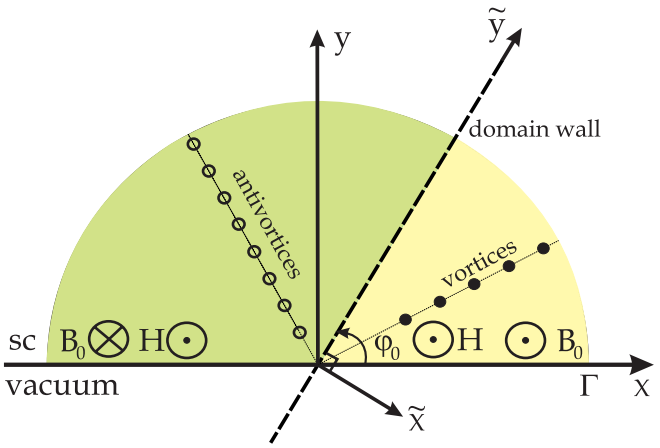

FIG. 8. (Color online) Schematic view of a F/S bilayer: a semi-infinite thin superconducting film and a straight domain wall (dashed line) oriented at a certain angle φ_0 with respect to the film edge Γ. B_0 is a stray field amplitude inside the domain, H is an external magnetic field, and the $\tilde{x}$ axis is chosen to be perpendicular to the domain wall. The vortex chain is shown by the solid circles, while the opened circles indicate the antivortices.

where α_1, γ_1, α_2, γ_2, and η are the variational parameters. The continuity condition for the wave function $\Psi(\mathbf{r})$ at $\varphi = \varphi_0$ gives the relation

$$\alpha_1(1+\gamma_1) = \alpha_2(1+\gamma_2). \tag{14}$$

For simplicity, we start with a particular case of the domain wall perpendicular to the film edge Γ ($\varphi_0 = \pi/2$). By substituting the expressions (12) and (13) into the functional (4) and carrying out the minimization over the variational parameters α_1, γ_1, α_2, γ_2, and η at a fixed amplitude B_0 of the magnetic stray field, we find the critical temperature T^*_{c3} versus the applied field H. The typical plot of the phase-transition line $T^*_{c3}(H)$ is presented in Fig. 9 by a solid line for $B_0 = 1.5H^{(0)}_{c2}$. One can see that by applying an external magnetic field H, we obtain an increase in the critical temperature T^*_{c3} of localized superconductivity due to the partial magnetic field compensation inside the domains.

As a next step, we restrict ourselves to the case $H = 0$ and analyze the dependence of the critical amplitude B^*_0 of the domain stray field corresponding to the superconductivity nucleation versus the φ_0 angle. By substituting the expressions (12) and (13) into Eq. (4), we carry out the minimization procedure over the variational parameters α_1, γ_1, α_2, γ_2, and η. The typical plot of the dependence $B^*_0(\varphi_0)$ shown in Fig. 3 by a dashed-dotted line (3) is in a good agreement with the solid line (2) derived within our numerical simulations discussed in the following.

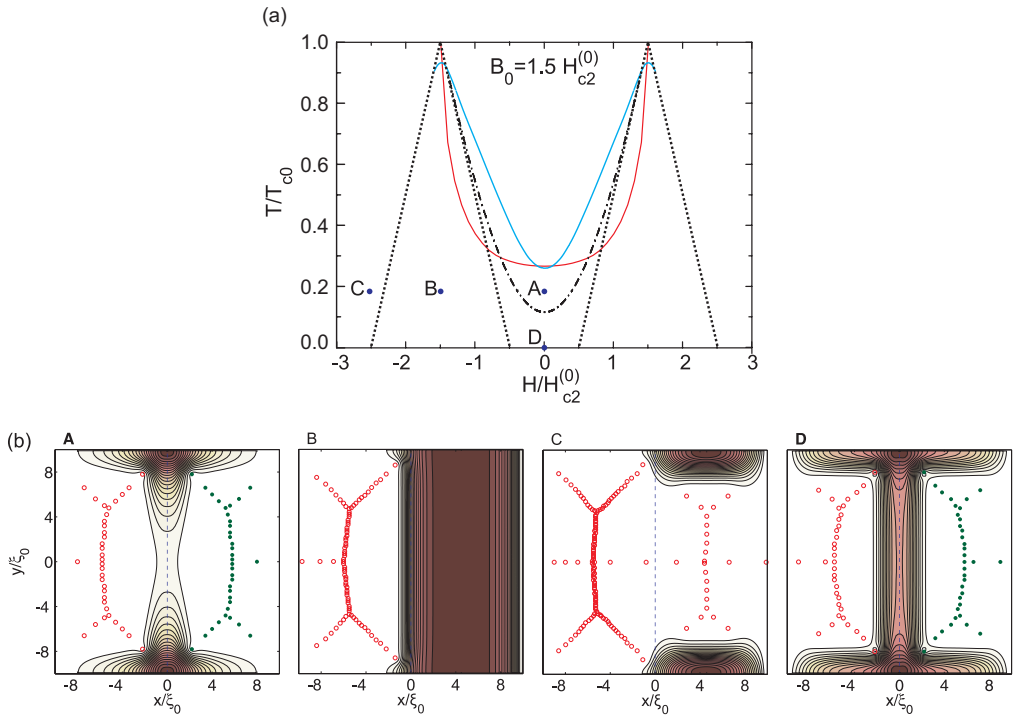

FIG. 9. (Color online) (a) Typical plots of the critical temperature $T^*_{c3}(H)$ for localized superconductivity in a thin-film semi-infinite F/S bilayer with a domain wall oriented perpendicular to the sample edge Γ ($\varphi_0 = \pi/2$, see Fig. 8). The solid line shows the results of our variational calculations, while the dashed line corresponds to our numerical simulations carried out for a rectangular superconducting film with lateral dimensions $20\xi_0 \times 20\xi_0$. The dotted lines correspond to the dependence of the shifted upper critical field of a bulk superconductor vs temperature: $T = T_{c0}\{1 - ||H| - B_0|/H^{(0)}_{c2}\}$, the dashed-dotted line shows the phase-transition line for a domain-wall superconductivity derived, e.g., in Refs. 5 and 6. Here, we take $B_0 = 1.5H^{(0)}_{c2}$. (b) Typical plots of superconducting OP distributions presented for different points on the H-T plane: A, B, C, and D, where the dashed line indicates the domain wall. The vortex chains are shown by the solid circles, while the antivortices are presented by open circles.

It is important to note that with the decrease in the angle φ_0, we clearly observe an increase in the field B_0^*. This increase obviously occurs due to a partial shrinking of the Cooper-pair wave function in analogy to the case of a superconducting wedge considered above. For small angles $\varphi_0 \to 0$, we find $B_0^*/H_{c2} \to 2.2$. In the case $\varphi_0 = \pi/2$ for an appropriate gauge choice, the problem of a half-infinite domain wall can be exactly mapped to the wedge problem for $\chi = \pi/2$. Indeed, for a domain wall perpendicular to the edge Γ, the GL functional is symmetric with respect to the parity transformation $x \to -x$ and, thus, the OP wave functions are either odd or even in the x variable. The even solutions corresponding to the energy minimum clearly satisfy the condition

$$\partial\Psi(\mathbf{r})/\partial x|_{x=0} = 0, \tag{15}$$

which coincides with that imposed for the superconducting wedge at the side with $\chi = \pi/2$. As a consequence, we find $B_0^*(\pi/2) = H_{c3}^{\mathrm{w}}(\pi/2) \simeq 2H_{c2}$. The variational parameters corresponding to this particular case should be taken as follows: $\alpha_1(\pi/2) = \alpha_2(\pi/2) = 0.14$, $\gamma_1(\pi/2) = \gamma_2(\pi/2) = -0.5$, $\eta(\pi/2) = 0.6$. However this mapping between the domain wall and the wedge, of course, does not hold exactly for $\varphi_0 \neq \pi/2$. Still, similarly to the wedge, the shrinking of the wave function at small angles φ_0 can result in the appearance of a vortex-free solution (see Sec. II C).

Two domain walls. The above variational results for the crossing domain wall and the sample edge remain valid also for two domain walls crossing at rather large angle $\varphi_0 \leqslant \pi/2$. Due to the symmetry of the magnetic field profile, this generalization is straightforward.

III. NUMERICAL SIMULATIONS

To confirm the findings obtained within the trial function approach, we proceed with the numerical analysis of the superconductivity nucleation in a thin-film F/S bilayer within the time-dependent GL formalism. Let us consider a superconducting thin-film rectangle in the plane (xy) of the Cartesian coordinate system (having the lateral dimensions $L \times W$) in the presence of a homogeneous external magnetic field $\mathbf{H}$ normal to the film plane and the steplike magnetic field $\mathbf{b}(\widetilde{x}) = \mathbf{z}_0 B_0\,\mathrm{sign}(\widetilde{x})$ of a straight domain wall oriented at a certain angle φ_0 with respect to the film edges $y = \pm W/2$ (see Fig. 10).

In order to obtain stationary OP distributions, we simulate the relaxation to an equilibrium state on the basis of the time-dependent GL model

$$-\eta\left[\hbar\frac{\partial}{\partial t} + 2ie\,\Phi(\mathbf{r})\right]\Psi(\mathbf{r}) = \alpha\,\Psi(\mathbf{r}) + \frac{\beta}{2}\,|\Psi(\mathbf{r})|^2\Psi(\mathbf{r}) + \frac{1}{4m}\left[-i\hbar\nabla - \frac{2e}{c}\mathbf{A}(\mathbf{r})\right]^2\Psi(\mathbf{r}),$$
$$\mathrm{div}\,\mathbf{j}_n(\mathbf{r}) = -\mathrm{div}\,\mathbf{j}_s(\mathbf{r}), \tag{16}$$

where the parameter η controls the rate of the OP relaxation, $\Phi(\mathbf{r})$ is the electrochemical potential, α and β are the parameters of the GL expansion, $\mathbf{j}_n(\mathbf{r}) = -\sigma\nabla\Phi(\mathbf{r})$, and

$$\mathbf{j}_s(\mathbf{r}) = \frac{e}{2m}\left\{\Psi(\mathbf{r})^*\left[-i\hbar\nabla - \frac{2e}{c}\mathbf{A}(\mathbf{r})\right]\Psi(\mathbf{r}) + \mathrm{c.c.}\right\} \tag{17}$$

are the densities of normal and superconducting currents, σ is a normal conductivity, and c.c. stands for complex conjugation. By focusing on the study of superconductivity nucleation, one can neglect the effect of vanishing supercurrents on the magnetic field distribution and consider a fixed vector potential profile corresponding to the magnetic field $B_z(\mathbf{r}) = H + b_z(\widetilde{x})$.

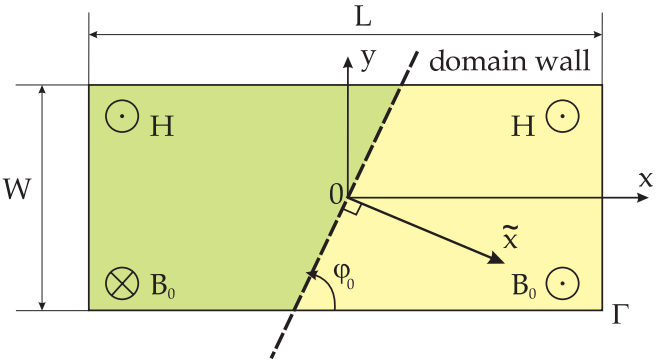

FIG. 10. (Color online) Schematic view of a F/S bilayer: a superconducting rectangle ($L \times W$) and a straight domain wall (dashed line) oriented at a certain angle φ_0 with respect to the edges $y = \pm W/2$. B_0 is a stray field amplitude inside the domain, H is an external magnetic field, the $\widetilde{x}$ axis is chosen to be perpendicular to the domain wall, and Γ is the film boundary.

The absence of normal current through the sample boundary imposes a boundary condition on the potential $\Phi(\mathbf{r})$:

$$\left.\frac{\partial\Phi(\mathbf{r})}{\partial\mathbf{n}}\right|_\Gamma = 0,$$

where $\mathbf{n}$ is a unit vector normal to the edge Γ of the sample. The calculations have been made for two types of boundary conditions on the superconducting OP wave function: (i) superconductor-insulator boundary condition

$$\left[-i\hbar\frac{\partial}{\partial\mathbf{n}} - \frac{2e}{c}\mathbf{A}_n\right]\Psi(\mathbf{r})\Big|_\Gamma = 0, \tag{18}$$

and (ii) superconductor-normal metal boundary condition

$$\Psi(\mathbf{r})\,|_\Gamma = 0. \tag{19}$$

To study the equilibrium phase diagram, we need all transient processes to be finished, which corresponds to zero electrochemical potential $\Phi(\mathbf{r}) = 0$ and zero time derivatives $\partial\Psi(\mathbf{r},t)/\partial t = 0$. In our calculations, we stopped the simulation procedure when the maximum of the electrochemical potential reaches the accuracy of the numerical computations ($10^{-15} \times \hbar|e|\alpha_0/2m\sigma\beta$ in the dimension units), where $\alpha_0 = |\alpha(T = 0)|$. The calculations have been carried out for a grid size $0.2\xi_0 \times 0.2\xi_0$ and $\eta = 10 \times m\sigma\beta/\hbar e^2$. The time interval between two subsequent iterations was chosen as follows: $0.01 \times m\sigma\beta/e^2\alpha_0$.

Let us start with the simplest case of a superconducting square ($L = W = 20\xi_0$) placed only in a homogeneous

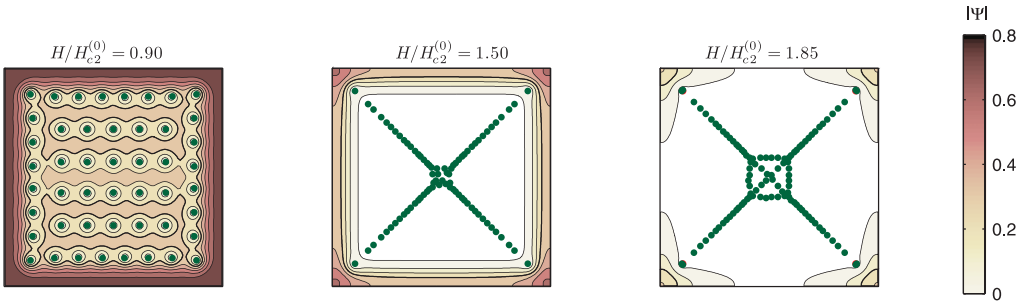

FIG. 11. (Color online) The OP distribution in a superconducting square ($20\xi_0 \times 20\xi_0$) in an increasing external magnetic field H. The boundary condition (18) was imposed on the Ψ function. Solid circles show the vortex chains.

magnetic field H. We consider here the boundary conditions for the Ψ function in the form (18). By varying the external field H, we study the evolution of the OP distribution $\Psi(x,y)$ in the superconducting square (see Fig. 11). One can see that the Cooper-pair wave function remains nonzero in the vicinity of the sample corners at the field above H_{c3}. Obviously, the corresponding nuclei at the corners can be considered separately only for rather large L values, well exceeding the nucleus size. In this case, each nucleus describes the OP distribution in a superconducting wedge with a corner angle $\pi/2$. The corresponding nucleation field $H_{c3}^{w} \simeq 2H_{c2}$ appears to be in a good agreement with the results of our variational analysis in Sec. II D. Our numerical simulations also give evidence for the appearance of the vortex chains introduced in the above consideration. These chains outgo from all four wedge vertices along the corresponding bisectrices (see Fig. 11).

We continue with the numerical analysis of the superconductivity nucleation in a superconducting rectangle $L \times W$ affected in the field of a straight domain wall. In order to suppress the superconductivity nucleation near the sample corners, we use mixed boundary conditions for the Ψ function: the conditions (18) and (19) are taken at the edges $y = \pm W/2$ and $x = \pm L/2$, respectively. Shown in Fig. 12 is the transformation of the OP distribution for a square with $L = W = 20\xi_0$ $\varphi_0 = \pi/2$ caused by the increase in the amplitude B_0 inside the domain. The numerical results are in a full agreement with our analytical findings in Sec. II D: (i) the superconductivity is localized near the crossing of the domain wall and the sample edges $y = \pm W/2$ and survives up to the critical value $B_0^* = H_c^{w} \simeq 2H_{c2}$; (ii) we observe the vortex (antivortex) chains outgoing from the crossing points of the superconducting channels.

By applying an external magnetic field H, we find out the phase diagram for localized superconducting states. For a particular case $B_0 = 1.5H_{c2}^{(0)}$, the corresponding phase-transition line is shown in Fig. 9 by the dashed line. We also observe the transition lines corresponding to the bulk superconductivity (dotted line in Fig. 9) and to the domain-wall superconductivity (dotted-dashed line in Fig. 9). Typical contour plots of the OP distributions for different parts of the phase diagram (see Fig. 9) illustrate the switching between the bulk and localized superconductivity nucleation.

In the limit of zero external field H, we have also analyzed the dependence of the critical field amplitude B_0^* on the φ_0 angle for the sample sizes $L = 30\xi_0$ and $W = 15\xi_0$. The typical plot of the dependence $B_0^*(\varphi_0)$ is shown in Fig. 3 by a solid line (2). Both for small and large corner angles, the numerical dependence is in a good agreement with the results of the variational analysis carried out in Sec. II D. Typical contour plots of the Cooper-pair wave function presented in Fig. 13 show the transformation of the vortex patterns with the changing φ_0 angle.

Let us focus on the vortex (antivortex) arrangements presented in Figs. 9, 11, 12, and 13. Near the crossing points of the superconducting channels, the vortex patterns obtained from our numerical simulations appear to be in a good agreement with the variational predictions for the infinite superconducting channels (see Sec. II) where the vortices (antivortices) form the vortex (antivortex) chains. Far from these crossing points, the vortex distributions are more

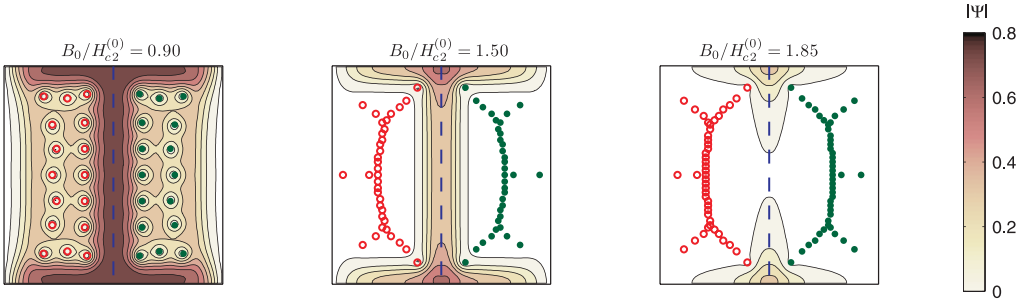

FIG. 12. (Color online) The OP distribution in a superconducting square ($20\xi_0 \times 20\xi_0$) for an increasing amplitude B_0 of the magnetic stray field in the domains and $\varphi_0 = \pi/2$. The boundary condition (19) was used for the Ψ function in order to suppress the superconductivity nucleation near the corners of the sample. The vortex and antivortex chains are shown by solid and open circles, respectively.

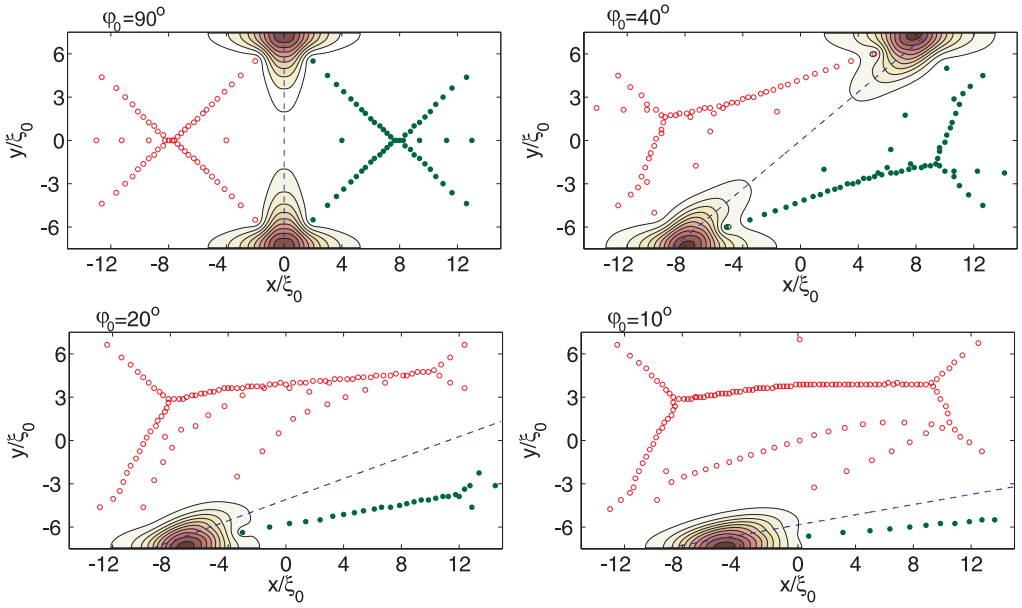

FIG. 13. (Color online) Typical contour plots of the superconducting OP distributions for different φ_0 angles: 90°, 40°, 20°, and 10°. The vortex and antivortex chains are shown by the solid and open circles, respectively.

complicated and strongly depend on the sample geometry and corresponding boundary conditions for the Cooper-pair wave function.

IV. CONCLUSION

To sum up, we have investigated the distinctive features of superconducting OP nucleation for the interacting superconducting channels in strong magnetic field $H > H_{c2}$. We have studied three generic problems: (i) the OP nucleation between two superconductor/vacuum boundaries forming a superconducting wedge; (ii) the OP nucleation between domain wall and the sample edge; and (iii) the OP nucleation between two domain walls. We have shown that in all these cases, the crossing of localized modes results in the increase in the superconducting critical temperature. Using both numerical and variational analysis of these problems, we have developed a description of the interference phenomena which govern the structure of the OP patterns. The resulting critical temperature enhancement and its magnetic field dependence should be observable in resistive measurements of hybrid F/S structures.

ACKNOWLEDGMENTS

This work was supported by the Russian Fund for Basic Research, RAS, under the Program "Quantum Physics of Condensed Matter," Russian Agency of Education under the Federal Target Program "Scientific and Educational Personnel of Innovative Russia in 2009–2013," and by the Dynasty Foundation.

[1] A. I. Buzdin, Rev. Mod. Phys. **77**, 935 (2005).
[2] A. Yu. Aladyshkin, A. V. Silhanek, W. Gillijns, and V. V. Moshchalkov, Supercond. Sci. Technol. **22**, 053001 (2009).
[3] Yu. V. Kopaev, Fiz. Tverd. Tela **7**, 2907 (1965) [Sov. Phys.–Solid State **7**, 2360 (1966)].
[4] A. I. Buzdin, L. N. Bulaevskii, and S. V. Panyukov, Zh. Eksp. Teor. Fiz. **87**, 299 (1984) [Sov. Phys.–JETP **60**, 174 (1984)].
[5] A. I. Buzdin and A. S. Mel'nikov, Phys. Rev. B **67**, 020503(R) (2003).
[6] A. Yu. Aladyshkin, A. I. Buzdin, A. A. Fraerman, A. S. Mel'nikov, D. A. Ryzhov, and A. V. Sokolov, Phys. Rev. B **68**, 184508 (2003).
[7] A. Yu. Rusanov, M. Hesselberth, J. Aarts, and A. I. Buzdin, Phys. Rev. Lett. **93**, 057002 (2004).
[8] Z. Yang, M. Lange, A. Volodin, R. Szymczak, and V. Moshchalkov, Nat. Mater. **3**, 793 (2004).
[9] R. Werner, A. Yu. Aladyshkin, S. Guenon, J. Fritzsche, I. M. Nefedov, V. V. Moshchalkov, R. Kleiner, and D. Koelle, Phys. Rev. B **84**, 020505(R) (2011).
[10] D. Saint-James and P. G. de Gennes, Phys. Lett. **7**, 306 (1963).
[11] D. Saint-James, G. Sarma, and E. J. Thomas, *Type-II Superconductivity* (Pergamon, Oxford, 1969).
[12] A. Houghton and F. B. McLean, Phys. Lett. **19**, 172 (1965).
[13] A. P. van Gelder, Phys. Rev. Lett. **20**, 1435 (1968).
[14] A. Yu. Simonov, A. S. Mel'nikov, and S. V. Sharov, Fiz. Nizk. Temp. **15**, 1206 (1989) [Low. Temp. Phys. **15**, 1206 (1989)].
[15] V. M. Fomin, J. T. Devreese, and V. V. Moshchalkov, Europhys. Lett. **42**, 553 (1998); **46**, 118(E) (1999).
[16] F. Brosense, V. M. Fomin, J. T. Devreese, and V. V. Moshchalkov, Solid State Commun. **144**, 494 (2007).
[17] S. N. Klimin, V. M. Fomin, J. T. Devreese, and V. V. Moshchalkov, Solid State Commun. **111**, 589 (1999).

[18] V. A. Schweigert and F. M. Peeters, Phys. Rev. B **60**, 3084 (1999).
[19] V. Bonnaillie-Noël, C. R. Math. **336**, 135 (2003).
[20] V. Bonnaillie-Noël, Asymptotic Analysis **41**, 215 (2005).
[21] V. Bonnaillie-Noël and M. Dauge, Ann. H. Poincare **7**, 899 (2006).
[22] H. T. Jadallah, J. Math. Phys. B **42**, 4101 (2001).
[23] A. Yu. Aladyshkin and V. V. Moshchalkov, Phys. Rev. B **74**, 064503 (2006).
[24] A. Yu. Aladyshkin, D. A. Ryzhov, A. V. Samokhvalov, D. A. Savinov, A. S. Mel'nikov, and V. V. Moshchalkov, Phys. Rev. B **75**, 184519 (2007).